Meccanica
https://doi.org/10.1007/s11012-021-01371-x

Fractional order models for the homogenization and wave propagation analysis in periodic elastic beams

Sansit Patnaik · John P. Hollkamp · Sai Sidhardh · Fabio Semperlotti

Received: 26 December 2020 / Accepted: 28 April 2021

Abstract The advancement of manufacturing techniques has led to a rapid increase in the design and fabrication of periodic and architectured materials for a variety of dynamics and wave manipulation applications. Classical low-frequency homogenization techniques have been popular and invaluable tools to facilitate the numerical simulation of these systems, although their application is naturally limited to the long-wavelength regime. As a result, scattering dominated features, such as the occurrence of frequency band-gaps, cannot be captured by these models. Indeed, the first band-gap typically marks the approximate limit of validity of low-frequency homogenization approaches. Abandoning the use of this approach allows recovering the detailed dynamic behavior due to the geometric features of the periodic units, but it also comes at a significant increase in computational cost. In this study, we leverage the use of fractional operators to revisit the classical low-frequency homogenization approaches and explore their possible extension beyond the initial band-pass (low-frequency) regime. Remarkably, the resulting fractional-order homogenization approach is capable of representing the dynamic behavior of periodic structures within the first few frequency band-gaps. In particular, we apply the fractional approach to model elastic wave propagation in a bi-material periodic beam which serves as an idealization of a one-dimensional elastic metamaterial. The use of the fractional operator formalism allows casting the classical integer-order wave equation with spatially-variable coefficients, typical of an inhomogeneous beam, into a fractional-order differential equation with constant coefficients. Thus, the spatial heterogeneity of the periodic system is accounted for via the order of the fractional derivative. The fractional-order governing equation is obtained via variational principles, starting from fractional-order kinematic relations. It is found that the resulting fractional differential model of the heterogeneous system has, in its most general form, a complex valued and frequency-dependent order. The results from the fractional order model are compared with those obtained from the classical wave equation in order to assess the validity of the approach and its performance. The dynamic analysis is carried out at both band-gap and band-pass regimes showing a good agreement with results from traditional methodologies.

Keywords Fractional calculus · Homogenization · Periodic media · Elastic metamaterials · Frequency band-gaps

S. Patnaik · J. P. Hollkamp · S. Sidhardh · F. Semperlotti (✉)
Ray W. Herrick Laboratories, School of Mechanical Engineering, Purdue University, West Lafayette, IN 47907, USA
e-mail: fsemperl@purdue.edu

Published online: 15 May 2021

1 Introduction

The rapid growth of the fields of periodic and architectured materials has further highlighted the need for accurate and efficient computational methods capable of predicting their dynamic behavior. Many of these media exploit the periodicity of certain structural features (e.g. the distribution of either material or geometric properties) to achieve a global dynamic behavior that would not be achievable in classical homogeneous material systems, such as metals or polymers. These materials are typically assembled by repeating periodically in space the smallest unit element, called the fundamental unit cell, that captures in itself all the distinctive constitutive features of the medium. When these periodic structures operate in a subwavelength frequency regime (the so-called metamaterial regime), they can exhibit unique wave-guiding characteristics including wave shaping, collimation, focusing, and steering [1–5].

Over the past few decades, several methods have been proposed to simulate the dynamics of these periodic structures. Some examples include, but are not limited to, model-order reduction techniques [6, 7], finite difference methods [8, 9], quadrature based methods [10, 11], finite element methods [12, 13], and plane-wave expansion methods [14, 15]. From a high-level perspective, all these approaches are characterized by a process of discretization of the system in either space or time. While these techniques have found good success and are still widely used, they are subject to limitations that impose an implicit trade-off between accuracy and computational time. Further, there are specific types of media for which the discretization process leads rapidly to computational resources that are beyond available capabilities. Examples of these media include multi-scale inhomogeneities such as those present in complex microstructures, porous and fractal media.

A very powerful alternative that is not subject to the same computational costs of discretized methods is offered by homogenization techniques [16–20] which eliminate the spatial dependence of the material parameters by replacing them with so-called effective parameters. Broadly speaking, there are two different approaches to classical homogenization: low-frequency approaches and high-frequency approaches. In classical low-frequency homogenization procedures, the inhomogeneous medium is replaced by a homogeneous one characterized by constant and uniform material properties capable of representing the behavior of the original material as a whole. These homogenized properties facilitate the use of continuum theory for the efficient prediction of the dynamic response of the complex medium. While these homogenization techniques have long been a powerful approach to model media having complex and inhomogeneous structure, they encounter some important limitations stemming from certain intrinsic assumptions at the basis of the method. In periodic structures, the classical low-frequency homogenization approaches fail to predict the existence and the location of frequency band-gaps, which are due to multiple scattering from the heterogeneous inclusions in the shorter wavelength regime (often indicated as the phononic regime). This is not surprising since the homogenized material properties can be representative of the actual heterogeneous medium only in a range where the wavelength of the propagating wave is sufficiently larger (typically by, at least, a factor of 2) than the characteristic dimension of the microstructural features [16, 19, 20]. This shortcoming was addressed by high-frequency approaches where an asymptotic multiple scale expansion of the homogenized material properties is used to capture some aspects of the microstructural features [17, 18]. Despite providing a very successful approach to broadband homogenization (apparently covering both material regimes), some limitations of the high-frequency approach follows from its theoretical formulation and the associated computational cost.

Independently of the specific approach, homogenization formulations intrinsically perform averaging operations of the spatially varying material properties and leverage specifically designed convoluted kernels to obtain either the homogenized material properties (in low-frequency approaches) or corrections to the first-order homogenized properties (in the high-frequency approaches). It is indeed this underlying convolution approach that motivated the present investigation and the corresponding reformulation of the homogenization approach via a class of differ-integral operators, known as fractional-order operators. As discussed in the following, fractional order operators are based on convolutions with power-law kernels, hence suggesting a natural application to homogenization problems. In recent years, fractional calculus has emerged as a powerful mathematical tool

to model a variety of complex physical phenomena. Fractional-order operators allow for the differentiation and integration to any real or complex order, are intrinsically multiscale, and provide a natural way to account for several complex physical mechanisms (e.g. nonlocal effects, medium heterogeneity, and memory effects) [21]. These characteristics of fractional operators have led to a surge of interest in fractional calculus and its application to the simulation of several physical problems. Areas that have seen the largest number of applications include the formulation of constitutive equations for viscoelastic materials [22, 23], model-order reduction of lumped parameter systems [24], modeling of nonlocal elasticity [25–36], phenomenological homogenized models [37–40], and transport processes in complex media [41–45].

As mentioned above, the differ-integral nature of fractional-order operators allows them to model spatial and temporal scale effects. While time fractional operators enable memory effects (i.e., the response of a system is a function of its past history), space fractional operators can account for medium heterogeneity, nonlocal effects and scale effects. In other terms, while temporal fractional derivatives physically represent damping and dissipation that occur in lossy or viscoelastic materials, spatial fractional derivatives are indicative of attenuation in systems that potentially are still conservative. That is, space fractional derivatives are ideal tools to capture frequency band-gaps in which attenuation is due to multiple back scattering and not to energy dissipation. This discussion suggests that fractional calculus can serve as a powerful mathematical tool for the homogenization and analysis of complex heterogeneous and periodic structures. In fact, recently, a handful of studies have started exploring this application of fractional calculus [38, 41]. In [38], Hollkamp et al. used space-fractional operators to obtain the homogenized equations governing the dynamic response of heterogeneous bi-material rods. The most notable result of this study was the validity of these equations beyond the classical homogenization (long wavelength) limit and their resulting ability to capture the response within, at least, the first frequency band-gap. In [38], the governing equations were numerically solved using a finite difference scheme that, while effective, was sensitive to instabilities due to the complex valued order of the fractional operators.

In this work, we perform a preliminary assessment on the use of fractional calculus as a homogenization technique to periodic systems while concurrently developing accurate and stable numerical techniques for complex valued fractional-order differential equations (which describe the resulting fractional-order homogenized media). The proposed fractional-order technique is more akin to the class of low-frequency approaches, in the sense that it replaces the spatially-varying material properties (or equivalently, the elastodynamic equation with spatially-varying coefficients) with homogenized material properties (or equivalently, constant coefficient elastodynamic equation). From a high level perspective, this study focuses on the generalization of the approach presented in [38] by pursuing two main objectives: (1) the extension of the underlying theoretical formulation to model the flexural response of periodic Euler–Bernoulli beams, particularly within the frequency band-gaps, and (2) the development of more efficient computational approaches for the solution of fractional complex-order differential equations. To achieve these two objectives we will first derive the fractional-order governing equations of an Euler–Bernoulli periodic beam by means of variational principles. Then, we will derive the dispersion relations of the fractional-order beam and use it to obtain the equivalent fractional order capable of capturing the response of the heterogeneous system. Finally, we will present a Ritz fractional-order finite element method (f-FEM) for complex-order equations and use it to simulate the steady-state response of the fractional-order beam. Fractional-order FEMs have been developed in the literature using Galerkin [46], Petrov–Galerkin [47] and very recently, Ritz-based methods [48]. However, it appears that none of these studies have addressed the solution of complex valued fractional-order equations. We anticipate that the f-FEM developed in this study is robust and capable of admitting both real and complex valued fractional-orders. The results obtained via the f-FEM establish that the fractional-order homogenization technique presents excellent predictions for the response of the periodic beam in the first band-gap and fairly good predictions within the second band-gap. Further, we also use these results to compare the fractional-order approach with classical low-frequency and high-frequency homogenization techniques. The proposed fractional-order technique is more akin to the classical low-frequency approach, in

the sense that it replaces the spatially-varying material properties (or equivalently, the elastodynamic equation with spatially-varying coefficients) with homogenized material properties (or equivalently, constant coefficient elastodynamic equation).

The remainder of the paper is structured as follows: first, we obtain the dispersion relations for a periodic beam using the classical Euler–Bernoulli theory. Next, we present a fractional-order theory for modeling the response of heterogeneous beams. Finally, we obtain the fractional model parameters for the periodic beam and use these parameters in the f-FEM to obtain the response of the periodic beam at different forcing frequencies.

2 Governing equations and dispersion relations of the periodic beam

In this study, we use the dispersion relation obtained using the classical (integer-order) beam theory in order to obtain the fractional model parameters for the periodic beam. Note that the strategy to determine the fractional order in a fractional mechanics representation can follow different avenues depending on the underlying physics being captured. This topic is still an object of extensive research and a widespread consensus on general methodologies has not been reached yet. Nevertheless, the focus of this study is on the formulation and performance of the fractional order approach to model periodic systems, hence the generality of this method will not be affected by the strategy employed for the order determination.

In order to implement the approach mentioned above, we first derive the dispersion relations for the periodic beam by using the classical (integer-order) Euler–Bernoulli beam formulation. Recall that the Euler–Bernoulli formulation is valid only for slender beams, that is for beams with a length to thickness ratio greater than or equal to approximately 100 [49]. Consider an infinite periodic beam consisting of two isotropic sections #1 and #2 with different properties, as shown in Fig. 1. The length of the two layers are denoted L_1 and L_2, such that the lattice constant d of the beam is given by $d = L_1 + L_2$ (see Fig. 1). The coordinate system is chosen such that the origin lies on the interface between the two layers. It is immediate that layer #1 appears for $x \in [-L_1 + Nd, Nd]$, while layer #2 appears for $x \in [Nd, L_2 + Nd]$, where $N = \{0, \pm 1, \pm 2 \ldots\}$ is a set of integers. The Young's modulus, quadratic moment of inertia, density and area of cross-section of the layers are denoted by E_m, I_m, ρ_m and A_m, respectively. In the above $m \in \{1, 2\}$, where $m = 1$ denotes the first layer, while $m = 2$ denotes the second layer within the periodic beam.

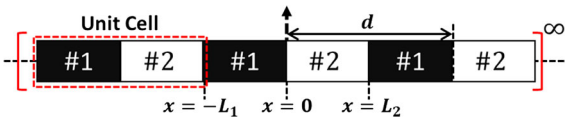

Fig. 1 Schematic of the periodic beam consisting of two sections having different material properties. Some characteristic dimensions are also shown

The governing equation of the Euler–Bernoulli beam in integer-order form is given by:

$$\frac{\partial^2}{\partial x^2}\left[E(x)I(x)\frac{\partial^2 w(x,t)}{\partial x^2}\right] + \rho(x)A(x)\frac{\partial^2 w(x,t)}{\partial t^2} = 0 \tag{1}$$

where $w(x, t)$ is the deflection of the mid-plane of the beam at a spatial location x and at the time instant t. In a periodic beam, the Young's modulus $E(x)$, the quadratic moment of inertia $I(x)$, the density $\rho(x)$, and the area of the cross-section $A(x)$ are periodic functions of the spatial location x with a period $d = L_1 + L_2$, as discussed above. Although the beam properties are a periodic function of the spatial location x, they are isotropic within each individual section. This latter consideration allows for the simplification of Eq. (1) to the following:

$$E_m I_m \frac{\partial^4 w(x,t)}{\partial x^4} + \rho_m A_m \frac{\partial^2 w(x,t)}{\partial t^2} = 0 \tag{2}$$

where $m = 1 \forall x \in [-L_1 + Nd, Nd]$ and $m = 2 \forall x \in [Nd, L_2 + Nd]$. Using the method of separation of variables we decompose $w(x, t)$ in the standard form $w(x,t) = W(x)\mathrm{e}^{-\mathrm{i}\omega t}$ involving the product of decoupled spatial and temporal functions. Note that ω is the angular frequency and $\mathrm{i} = \sqrt{-1}$. Substituting $w(x, t)$ in Eq. (2) results in the following expression for $W(x)$:

$$W(x) = A_{m1}\mathrm{e}^{\beta_m x} + A_{m2}\mathrm{e}^{-\beta_m x} + A_{m3}\mathrm{e}^{\mathrm{i}\beta_m x} + A_{m4}\mathrm{e}^{-\mathrm{i}\beta_m x} \tag{3a}$$

$$\beta_m = \left[\frac{\rho_m A_m \omega^2}{E_m I_m}\right]^{\frac{1}{4}} \tag{3b}$$

where $m \in \{1,2\}$ and A_{m1}, A_{m2}, A_{m3}, and A_{m4} are either real or complex constants. Further, it appears from Eq. (2) that the coefficients of the beam governing differential equations are periodic in nature. Using the Floquet theorem for the periodic beam, it can be shown that the displacement, slope, bending moment, and shear force are quasi-periodic across adjoining cells. It follows that:

$$W(x) = \mathrm{e}^{\lambda d} W(x-d) \forall x \in (-\infty, \infty) \tag{4}$$

where λ is the Floquet wave number which can be either real or complex.

The dispersion relations for the periodic beam can now be derived by establishing a relationship between the set of eight constants A_{m1}, A_{m2}, A_{m3}, and A_{m4}. Imposing the continuity of displacement, slope, bending moment, and shear force at $x = 0$ (i.e. at the interface between the two layers within a unit cell) results in the following set of four equations:

$$\begin{aligned} &A_{11} + A_{12} + A_{13} + A_{14} \\ &\quad = A_{21} + A_{22} + A_{23} + A_{24} \end{aligned} \tag{5a}$$

$$\begin{aligned} &\beta_1 A_{11} - \beta_1 A_{12} + \mathrm{i}\beta_1 A_{13} - \mathrm{i}\beta_1 A_{14} \\ &\quad = \beta_2 A_{21} - \beta_2 A_{22} + \mathrm{i}\beta_2 A_{23} - \mathrm{i}\beta_2 A_{24} \end{aligned} \tag{5b}$$

$$\begin{aligned} &E_1 I_1 \left[\beta_1^2 A_{11} + \beta_1^2 A_{12} - \beta_1^2 A_{13} - \beta_1^2 A_{14}\right] \\ &\quad = E_2 I_2 \left[\beta_2^2 A_{21} + \beta_2^2 A_{22} - \beta_2^2 A_{23} - \beta_2^2 A_{24}\right] \end{aligned} \tag{5c}$$

$$\begin{aligned} &E_1 I_1 \left[\beta_1^3 A_{11} - \beta_1^3 A_{12} - \mathrm{i}\beta_1^3 A_{13} + \mathrm{i}\beta_1^3 A_{14}\right] \\ &\quad = E_2 I_2 \left[\beta_2^3 A_{21} - \beta_2^3 A_{22} - \mathrm{i}\beta_2^3 A_{23} + \mathrm{i}\beta_2^3 A_{24}\right] \end{aligned} \tag{5d}$$

An additional set of four relations are established by using the Floquet relations in Eq. (4) in order to relate the different physical variables at $x = -L_1$ and at $x = L_2$. This gives:

$$\begin{aligned} &A_{11}\mathrm{e}^{\lambda d - \beta_1 L_1} + A_{12}\mathrm{e}^{\lambda d + \beta_1 L_1} + A_{13}\mathrm{e}^{\lambda d - \mathrm{i}\beta_1 \mathrm{L}_1} + A_{14}\mathrm{e}^{\lambda d + \mathrm{i}\beta_1 \mathrm{L}_1} \\ &\quad = A_{21}\mathrm{e}^{\beta_2 L_2} + A_{22}\mathrm{e}^{-\beta_2 L_2} + A_{23}\mathrm{e}^{\mathrm{i}\beta_2 \mathrm{L}_2} + A_{24}\mathrm{e}^{-\mathrm{i}\beta_2 \mathrm{L}_2} \end{aligned} \tag{6a}$$

$$\begin{aligned} &\beta_1 A_{11}\mathrm{e}^{\lambda d - \beta_1 L_1} - \beta_1 A_{12}\mathrm{e}^{\lambda d + \beta_1 L_1} \\ &\quad + \mathrm{i}\beta_1 A_{13}\mathrm{e}^{\lambda d - \mathrm{i}\beta_1 \mathrm{L}_1} - \mathrm{i}\beta_1 A_{14}\mathrm{e}^{\lambda d + \mathrm{i}\beta_1 \mathrm{L}_1} \\ &\quad = \beta_2 A_{21}\mathrm{e}^{\beta_2 L_2} - \beta_2 A_{22}\mathrm{e}^{-\beta_2 L_2} + \mathrm{i}\beta_2 A_{23}\mathrm{e}^{\mathrm{i}\beta_2 \mathrm{L}_2} - \mathrm{i}\beta_2 A_{24}\mathrm{e}^{-\mathrm{i}\beta_2 \mathrm{L}_2} \end{aligned} \tag{6b}$$

$$\begin{aligned} &E_1 I_1 \left[\beta_1^2 A_{11}\mathrm{e}^{\lambda d - \beta_1 L_1} + \beta_1^2 A_{12}\mathrm{e}^{\lambda d + \beta_1 L_1}\right. \\ &\quad \left. - \beta_1^2 A_{13}\mathrm{e}^{\lambda d - \mathrm{i}\beta_1 \mathrm{L}_1} - \beta_1^2 A_{14}\mathrm{e}^{\lambda d + \mathrm{i}\beta_1 \mathrm{L}_1}\right] \\ &\quad = E_2 I_2 \left[\beta_2^2 A_{21}\mathrm{e}^{\beta_2 L_2} + \beta_2^2 A_{22}\mathrm{e}^{-\beta_2 L_2}\right. \\ &\quad \left. - \beta_2^2 A_{23}\mathrm{e}^{\mathrm{i}\beta_2 \mathrm{L}_2} - \beta_2^2 A_{24}\mathrm{e}^{-\mathrm{i}\beta_2 \mathrm{L}_2}\right] \end{aligned} \tag{6c}$$

$$\begin{aligned} &E_1 I_1 \left[\beta_1^3 A_{11}\mathrm{e}^{\lambda d - \beta_1 L_1} - \beta_1^3 A_{12}\mathrm{e}^{\lambda d + \beta_1 L_1}\right. \\ &\quad \left. - \mathrm{i}\beta_1^3 A_{13}\mathrm{e}^{\lambda d - \mathrm{i}\beta_1 \mathrm{L}_1} + \mathrm{i}\beta_1^3 A_{14}\mathrm{e}^{\lambda d + \mathrm{i}\beta_1 \mathrm{L}_1}\right] \\ &\quad = E_2 I_2 \left[\beta_2^3 A_{21}\mathrm{e}^{\beta_2 L_2} - \beta_2^3 A_{22}\mathrm{e}^{-\beta_2 L_2}\right. \\ &\quad \left. - \mathrm{i}\beta_2^3 A_{23}\mathrm{e}^{\mathrm{i}\beta_2 \mathrm{L}_2} + \mathrm{i}\beta_2^3 A_{24}\mathrm{e}^{-\mathrm{i}\beta_2 \mathrm{L}_2}\right] \end{aligned} \tag{6d}$$

The Eqs. (5,6) are combined to form a set of eight homogeneous equations of the form $[T]\{X\} = 0$, where $X = \{A_{11} A_{12} A_{13} A_{14} - A_{21} - A_{22} - A_{23} - A_{24}\}^T$ is a vector containing the eight constants. The matrix $[T]$ is obtained as:

$$[T] = \begin{bmatrix} 1 & 1 & 1 & 1 & 1 & 1 & 1 & 1 \\ 1 & -1 & \mathrm{i} & -\mathrm{i} & \tilde{\beta} & -\tilde{\beta} & \mathrm{i}\tilde{\beta} & -\mathrm{i}\tilde{\beta} \\ 1 & 1 & -1 & -1 & \tilde{Z}\tilde{\beta}^2 & \tilde{Z}\tilde{\beta}^2 & -\tilde{Z}\tilde{\beta}^2 & -\tilde{Z}\tilde{\beta}^2 \\ 1 & -1 & -\mathrm{i} & \mathrm{i} & \tilde{Z}\tilde{\beta}^3 & -\tilde{Z}\tilde{\beta}^3 & -\mathrm{i}\tilde{Z}\tilde{\beta}^3 & \mathrm{i}\tilde{Z}\tilde{\beta}^3 \\ \kappa\mathrm{e}^{-\beta_1 L_1} & \kappa\mathrm{e}^{\beta_1 L_1} & \kappa\mathrm{e}^{-\mathrm{i}\beta_1 \mathrm{L}_1} & \kappa\mathrm{e}^{\mathrm{i}\beta_1 \mathrm{L}_1} & \mathrm{e}^{\beta_2 L_2} & \mathrm{e}^{-\beta_2 L_2} & \mathrm{e}^{\mathrm{i}\beta_2 \mathrm{L}_2} & \mathrm{e}^{-\mathrm{i}\beta_2 \mathrm{L}_2} \\ \kappa\mathrm{e}^{-\beta_1 L_1} & -\kappa\mathrm{e}^{\beta_1 L_1} & \mathrm{i}\kappa\mathrm{e}^{-\mathrm{i}\beta_1 \mathrm{L}_1} & -\mathrm{i}\kappa\mathrm{e}^{\mathrm{i}\beta_1 \mathrm{L}_1} & \tilde{\beta}\mathrm{e}^{\beta_2 L_2} & -\tilde{\beta}\mathrm{e}^{-\beta_2 L_2} & \mathrm{i}\tilde{\beta}\mathrm{e}^{\mathrm{i}\beta_2 \mathrm{L}_2} & -\mathrm{i}\tilde{\beta}\mathrm{e}^{-\mathrm{i}\beta_2 \mathrm{L}_2} \\ \kappa\mathrm{e}^{-\beta_1 L_1} & \kappa\mathrm{e}^{\beta_1 L_1} & -\kappa\mathrm{e}^{-\mathrm{i}\beta_1 \mathrm{L}_1} & -\kappa\mathrm{e}^{\mathrm{i}\beta_1 \mathrm{L}_1} & \tilde{Z}\tilde{\beta}^2\mathrm{e}^{\beta_2 L_2} & \tilde{Z}\tilde{\beta}^2\mathrm{e}^{-\beta_2 L_2} & -\tilde{Z}\tilde{\beta}^2\mathrm{e}^{\mathrm{i}\beta_2 \mathrm{L}_2} & -\tilde{Z}\tilde{\beta}^2\mathrm{e}^{-\mathrm{i}\beta_2 \mathrm{L}_2} \\ \kappa\mathrm{e}^{-\beta_1 L_1} & -\kappa\mathrm{e}^{\beta_1 L_1} & -\mathrm{i}\kappa\mathrm{e}^{-\mathrm{i}\beta_1 \mathrm{L}_1} & \mathrm{i}\kappa\mathrm{e}^{\mathrm{i}\beta_1 \mathrm{L}_1} & \tilde{Z}\tilde{\beta}^3\mathrm{e}^{\beta_2 L_2} & -\tilde{Z}\tilde{\beta}^3\mathrm{e}^{-\beta_2 L_2} & -\mathrm{i}\tilde{Z}\tilde{\beta}^3\mathrm{e}^{\mathrm{i}\beta_2 \mathrm{L}_2} & \mathrm{i}\tilde{Z}\tilde{\beta}^3\mathrm{e}^{-\mathrm{i}\beta_2 \mathrm{L}_2} \end{bmatrix} \tag{7}$$

where $\kappa = e^{\lambda d}, \tilde{\beta} = \beta_2/\beta_1$, and $\tilde{Z} = E_2 I_2 / E_1 I_1$. For a nontrivial solution to the displacement field of the periodic beam the determinant of the matrix $[T]$ must be set to zero. This yields the dispersion relation for the periodic beam as a fourth degree polynomial of the variable κ given as:

$$\mathcal{P}(\kappa) = a_4\kappa^4 + a_3\kappa^3 + a_2\kappa^2 + a_1\kappa + a_0 = 0 \tag{8}$$

where a_k are either real or complex constants. The roots of the above polynomial give the value of κ and subsequently the Floquet wave number λ.

Given the complex nature of the matrix $[T]$, we did not obtain explicit expressions for the wave number λ and instead adopted a numerical approach. We make a remark here pertaining to the numerical procedure of finding the roots of the above polynomial $\mathcal{P}(\kappa)$. Given the presence of exponentials within the matrix $[T]$, the coefficients of the characteristic polynomial $\mathcal{P}(\kappa)$ are highly conditioned, i.e., ratios of the coefficients of $\mathcal{P}(\kappa)$ are large. In such a case it was found that the use of numerical root-finding solvers results in erroneous solutions for κ. In order to extract the roots accurately, we exploit a certain symmetry within the periodic beam in order to factorize $\mathcal{P}(\kappa)$ into two quadratic polynomials.

Note that the continuity and the Floquet relations remain unchanged when the layers within the periodic beam are interchanged. More specifically, the formulation remains unchanged under the transformation: $L_2 \rightarrow -L_1$ and $L_1 \rightarrow -L_2$. Under this transformation $\beta_2 \rightarrow \beta_1$ and $\beta_1 \rightarrow \beta_2$. Using these transformations within the determinant leads to the fact that $a_0 = a_4$ and $a_1 = a_3$. Now, on dividing the polynomial $\mathcal{P}(\kappa)$ by the leading order coefficient a_4, it is immediate that $\mathcal{P}(\kappa)$ can be factorized into two quadratic polynomials in the following fashion:

$$\mathcal{P}(\kappa) \equiv (\kappa^2 + p_1\kappa + 1)(\kappa^2 + p_2\kappa + 1) = 0 \tag{9}$$

where the coefficients p_1 and p_2 are given as:

$$p_{1,2} = \frac{1}{2}\left[\frac{a_3}{a_4} \pm \sqrt{\left(\frac{a_3}{a_4}\right)^2 - 4\left(\frac{a_2}{a_4} - 2\right)}\right] \tag{10}$$

Using the factorized quadratic polynomials, the solutions for κ can now be found by using the standard results for obtaining the roots of quadratic polynomials:

$$\kappa_{1,2} = \frac{1}{2}\left[-p_1 \pm \sqrt{p_1^2 - 4}\right] \tag{11a}$$

$$\kappa_{3,4} = \frac{1}{2}\left[-p_2 \pm \sqrt{p_2^2 - 4}\right] \tag{11b}$$

The Floquet wave number can be found by taking the logarithm of the obtained values of κ:

$$\lambda_n = \frac{1}{d}\log(\kappa_n) \tag{12}$$

where $n = \{1, 2, 3, 4\}$. It follows from Eq. (11) that $\kappa_1\kappa_2 = 1$ and $\kappa_3\kappa_4 = 1$. Thus, in principle, $\lambda_2 = -\lambda_1 + iN_1\pi/d$ and $\lambda_4 = -\lambda_3 + iN_2\pi/d$ where N_1 and N_2 are integers. We choose $N_1 = 0$ and $N_2 = 0$ here and hence we take the principal logarithm in Eq. (12). Note that this does not affect the generality of the results and we will show that this results in a folding of the dispersion curves across the first (irreducible) Brillouin zone of the periodic beam. In the subsequent analysis, we consider a periodic beam consisting of aluminum and brass. The specific properties of the layer #1: Aluminum and layer #2: Brass are given in Table 1. The dispersion of flexural waves in this periodic beam is obtained using the above presented formalism and is shown in Fig. 2. Figure 2a plots the wave number versus frequency folded across the first Brillouin zone while Fig. 2b is the unfolded dispersion curve for the aluminum-brass rod. The frequency regions where $\Re(\lambda) \neq 0$, highlighted in the plots with a gray area, are the frequency band-gaps of the periodic aluminum-brass beam; that is, these are the frequency ranges where wave propagation will not

Table 1 Properties of the layers within the periodic beam

Material	Young's modulus (GPa)	Density (kg/m^3)	Length (m)	Thickness (m)	Width (m)
Aluminum	70	2700	1	0.005	0.005
Brass	110	8100	1	0.005	0.005

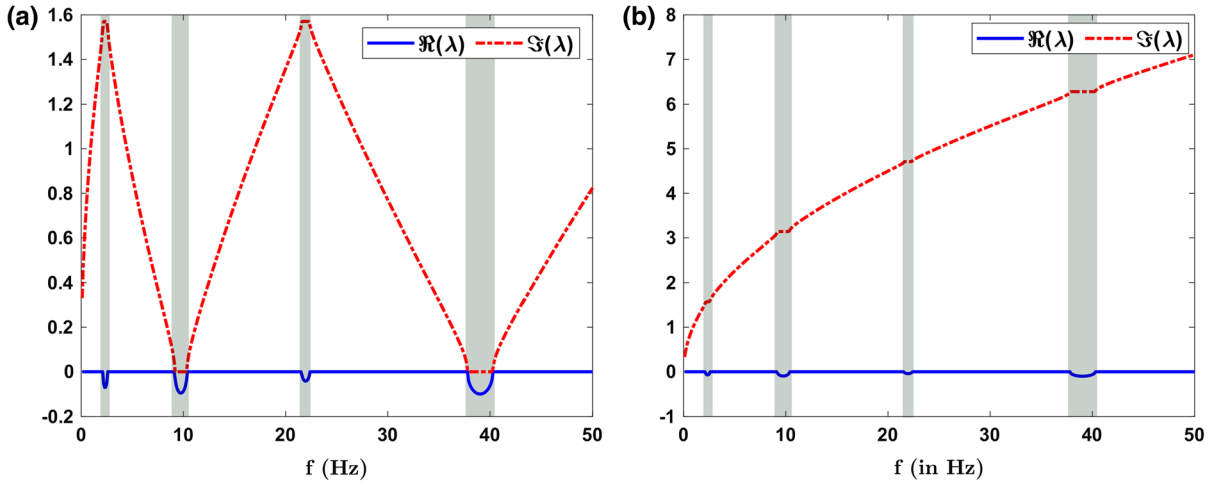

Fig. 2 Plot of the dispersion curve of the aluminum-brass periodic beam. **a** The dispersion curve is folded across the first Brillouin zone. **b** The unfolded dispersion curve of the periodic beam

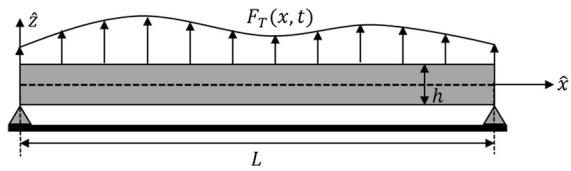

Fig. 3 Schematic of a linear elastic beam subject to a distributed transverse load $F_t(x,t)$

persist due to the scattering effects taking place on the local features of the unit cell.

3 Fractional-order model of the periodic beam

In this section, we develop the fractional-order model for the analysis of the periodic beam. As discussed in [38, 41], the fractional-order approach can be considered as a homogenization technique where the space-fractional operators capture the effect of inhomogeneities. Under the slender beam assumptions, a fractional-order analogue of the Euler–Bernoulli beam theory can be developed to model the displacement field of the homogenized beam subjected to transverse loads. The dimensions of the beam are $L \times b \times h$, where L is the length, b is the width, and h is the height, as illustrated in Fig. 3. The nonlocal axial strain $(\tilde{\epsilon})$ in the fractional-order beam is defined as [34, 48]:

$$\tilde{\epsilon}(x,z) = -zD_x^{\alpha}\left[\frac{\partial \tilde{w}(x,t)}{\partial x}\right] \tag{13}$$

where $\tilde{w}$ is the fractional-order homogenized transverse response of the beam. In this study, we consider only slender beams $(L/h = 200)$. Recall that, for slender beams $(L/h > 50)$, the rigidity to transverse shear forces is much higher when compared to the bending rigidity, therefore the contribution of the shear deformation is essentially negligible [34, 48, 49].

In the above equation, $D_x^{\alpha}(\cdot)$ is a space-fractional Riesz-Caputo (RC) derivative with order $\alpha \in (0,1)$ defined on the interval $x \in (0,L)$ as [34, 48]:

$$D_x^{\alpha}\Psi(x) = \frac{1}{2}\tilde{l}^{\alpha-1}\left[{}_0^C D_x^{\alpha}\Psi(x) - {}_x^C D_L^{\alpha}\Psi(x)\right] \tag{14}$$

where Ψ is an arbitrary function, and $\tilde{l}$ is a length-scale factor introduced to ensure dimensional consistency of the fractional-order derivative. ${}_0^C D_x^{\alpha}(\cdot)$ and ${}_x^C D_L^{\alpha}$ are the left- and right-handed Caputo derivatives to the order α, respectively. The interval of the RC fractional derivative $(0, L)$ defines the horizon of nonlocality of the fractional-order beam, i.e., the distance beyond which information is no longer accounted for within the fractional derivative. Note that the horizon of nonlocality in this study coincides with the length of the beam, which is different from [41] where a finite dimensional nonlocal horizon was defined. This difference in the selection of the size of the nonlocal horizon is consistent with the fact that this study deals with the response of an infinite heterogeneous beam (as opposed to [48] that focused on the response of

homogeneous and finite nonlocal beams). It follows that, while analysing an infinite beam the horizon of nonlocality would correspondingly extend over the entire beam, i.e., it would be infinite in nature. In this case, the nonlocal convolution (corresponding to the intervals of the RC derivative) would be performed over the interval $(-\infty, \infty)$. While it is possible to assume a finite length for the horizon of the fractional-order beam, we decided to choose the entire length of the beam as the horizon in order to reduce the number of fractional model parameters to one, that is the fractional-order α. As we will show in Sect. 4, the equivalence of the dispersion relations of the fractional-order model and integer-order model allows determining the value of a single parameter. We use this equivalence to fix the value of α. We merely note that this assumption on the infinite extent of the nonlocal horizon matches closely with the formulation proposed by Eringen *et al.* [50]. Note also that classical integer-order homogenization theories often result in integral averaging expressions over the entire domain of the solid [19]. Further, we emphasize here that, the use of the Caputo fractional derivatives in Eq. (13) leads to a frame-invariant formulation. Recall that the Caputo derivative of a constant function is zero, as for classical integer-order derivatives. This property does not hold true for all definitions of fractional derivatives [21]. In the context of frame invariance, this is a key point that ensures that no strain is accumulated in the 1D solid under translation [25, 30].

Further, the axial stress $(\tilde{\sigma})$ in the homogenized fractional-order beam is defined as:

$$\tilde{\sigma}(x,z) = \tilde{E}\tilde{\epsilon}(x,z) \tag{15}$$

where $\tilde{E}$ is the Young's modulus of the fractional-order beam. The thermodynamic consistency of the above constitutive equations has been discussed in detail in [51]. Using the above defined strain and stress fields, the total nonlocal potential energy of the fractional-order beam of volume Ω is obtained as:

$$\Pi = \frac{1}{2}\int_{\Omega} \tilde{\sigma}(x,z)\tilde{\epsilon}(x,z)\mathrm{d}V - \int_{L} F_T(x,t)\tilde{w}(x)\mathrm{d}x \tag{16}$$

where the second integral in the above expression corresponds to the work done by the transverse force $F_T(x,t)$ which is applied externally on a plane perpendicular to the mid-plane of the beam. We have also assumed that no body forces are applied. The kinetic energy of the beam is given as:

$$T = \frac{1}{2}\int_{\Omega} \tilde{\rho}\left(\frac{\partial \tilde{w}}{\partial t}\right)^2 \mathrm{d}V \tag{17}$$

Using the expressions for the potential and kinetic energy, the governing differential equations (GDE), the associated boundary conditions (BC), and the initial conditions (IC) necessary to determine the response of the fractional-order beam are obtained by using the generalized Hamilton's principle as:

$$\begin{aligned} \text{GDE}: \tilde{E}\tilde{I}\frac{\partial}{\partial x}\left[\mathfrak{D}_x^{\alpha}\left[D_x^{\alpha}\left(\frac{\partial \tilde{w}}{\partial x}\right)\right]\right] + \tilde{\rho}\tilde{A}\frac{\partial^2 \tilde{w}}{\partial t^2} \\ = F_T(x,t)\ \forall\ x \in (0,L) \cup t \in (0,\infty) \end{aligned} \tag{18a}$$

$$\text{BC}: \begin{cases} \tilde{E}\tilde{I}\left[\mathcal{I}_x^{1-\alpha} D_x^{\alpha}\left(\frac{\partial \tilde{w}(x,t)}{\partial x}\right)\right] = 0 \text{ or } \delta\left[\frac{\partial \tilde{w}(x,t)}{\partial x}\right] \\ \qquad = 0 \text{ at } x \in \{0,L\} \ \cup\ t \in (0,\infty) \\ \tilde{E}\tilde{I}\left[\mathfrak{D}_x^{\alpha} D_x^{\alpha}\left(\frac{\partial \tilde{w}(x,t)}{\partial x}\right)\right] = 0 \text{ or } \delta\tilde{w}(x,t) \\ \qquad = 0 \text{ at } x \in \{0,L\} \ \cup\ t \in (0,\infty) \end{cases} \tag{18b}$$

$$\begin{aligned} \text{IC: } \delta\tilde{w}(x,t) = 0 \text{ and } \delta\left(\frac{\partial \tilde{w}(x,t)}{\partial t}\right) \\ = 0 \text{ at } t = 0\ \cup\ x \in (0,L) \end{aligned} \tag{18c}$$

where $\tilde{I}$, $\tilde{\rho}$, and $\tilde{A}$ are the quadratic moment of inertia, density, and cross-sectional area of the fractional-order beam, respectively. The detailed steps leading to the above simplification can be found in [48] where a similar variational approach has been used in the context of slender fractional-order nonlocal structures. In Eq. (18), $\mathfrak{D}_x^{\alpha}(\cdot)$ is a Riesz-type Riemann-Liouville (R-RL) derivative of order α defined on the interval $x \in (0,L)$ as:

$$\mathfrak{D}_x^{\alpha}\Psi(x) = \frac{1}{2}\tilde{l}^{\alpha-1}\left[{}_0^{RL}D_x^{\alpha}\Psi(x) - {}_x^{RL}D_L^{\alpha}\Psi(x)\right] \tag{19}$$

where Ψ is an arbitrary function, and ${}_0^{RL}D_x^{\alpha}(\cdot)$ and ${}_x^{RL}D_L^{\alpha}(\cdot)$ are the left- and right-handed Riemann Liouville fractional-order derivatives, respectively. $\mathcal{I}_x^{1-\alpha}(\cdot)$ is a Reisz-type fractional integral defined in the following fashion:

$$\mathcal{I}^{1-\alpha}\Psi(x) = \frac{1}{2}\tilde{l}^{\alpha-1}\left[{}_0\mathcal{I}_x^{1-\alpha}\Psi(x) + {}_x\mathcal{I}_L^{1-\alpha}\Psi(x)\right] \quad (20)$$

where ${}_0\mathcal{I}_x^{1-\alpha}(\cdot)$ and ${}_x\mathcal{I}_L^{1-\alpha}(\cdot)$ are the left- and right-handed Riemann Liouville fractional-order integrals, respectively. Note that classical beam governing equations are recovered for $\alpha = 1$.

The above presented fractional-order beam model deserves a few additional remarks. First, note that the fractional-order formulation presented in this study follows from that presented in [48]. While this study is concerned with the homogenization of heterogeneous structures using fractional calculus, the study conducted in [48] focused primarily on the modeling of nonlocal beams. With regards to the latter remark and given the differ-integral definition of the fractional-order operators, we emphasize that the fractional-order formulation is capable of modeling both nonlocal elasticity as well as homogenized response of heterogeneous structures. We merely note that the modeling of the long-range cohesive forces in nonlocal elasticity can also be interpreted as a homogenization approach wherein the effect of a large number of points within a prescribed distance, known as the horizon of nonlocality, is accounted for in the continuum governing equations. Further, in contrast to [48] which focuses primarily on the static response of beams, this study focuses on the dynamic analysis of the fractional-order beam.

Next, we also emphasize that the set of linear operators describing the governing differential equations (18a–18c) of the beam are self-adjoint. This ensures that the system is positive definite independently of the boundary or loading conditions. Thus, the fractional-order approach presents a way to homogenize the response of heterogeneous structures while ensuring a self-adjoint positive definite system. As mentioned previously, this property leads to well-posed formulations free from boundary effects and inaccurate predictions, hence enabling the use of variational-principles to develop FE techniques for numerical simulations. This latter observation is of particular interest because the classical integral formulations of nonlocal beams available in literature have been shown to be ill-posed and leading to inaccurate (also called "paradoxical") predictions for certain boundary conditions [48, 52]. In conclusion, the proposed fractional-order approach is mathematically well-posed [48], causal [25, 41], frame-invariant [41], thermodynamically consistent [51], and satisfies strain compatibility [41]. These characteristics suggest that the proposed fractional-order approach is physically and mathematically consistent. The latter comment is critical because the literature on fractional continuum mechanics shows that not every fractional-order elastodynamic formulation is mathematically and physically consistent. Notably, there can be reformulations to the present approach based on recently proposed $\Lambda-$fractional derivatives. The interested reader can find detailed discussions on these operators in [53–55].

4 Fractional model parameters for the periodic beam

In order to apply the fractional-order beam model to the analysis of the dynamic response of the periodic beam, we must obtain the fractional model parameters, namely the order α and length scale $\tilde{l}$, corresponding to the periodic beam. While different strategies could be envision to accomplish this step, in this study we insist that the dispersion in the periodic beam obtained using the classical approach and the fractional-order approach are equivalent. The dispersion relations for the integer-order periodic beam were derived in Sect. 2. To obtain the dispersion relation of the fractional-order beam, we substitute the following ansatz in the homogeneous part of the fractional-order beam governing equation:

$$\tilde{w}(x,t) = A_1 e^{(\tilde{\lambda}x - i\omega t)} + A_2 e^{(\tilde{\lambda}x + i\omega t)} \quad (21)$$

where A_1 and A_2 are the amplitudes of the wave propagating in the positive and in the negative $\hat{x}$ direction, respectively. Further, $\tilde{\lambda}$ is the wave number of the wave and ω is the angular frequency. Note that the wave number $\tilde{\lambda}$ can be real or complex. Given the wave solution assumed in Eq. (21), the real and complex parts of the complex wave number $\tilde{\lambda}$ correspond to the attenuating and propagating component of the wave. Note that, the ansatz assumed in Eq. (21) is contrary to the standard form: $A_1 e^{i(\tilde{\lambda}x - \omega t)} + A_2 e^{i(\tilde{\lambda}x + \omega t)}$. We assumed the former expression in order to remain consistent with the form of the Floquet wave number assumed in Sect. 2.

It appears that the derivation of the dispersion relations requires the operation of the R-RL derivative and the RC derivative in Eq. (18) on the exponential functions in the assumed solution in Eq. (21). As mentioned previously, the R-RL and the RC derivatives in Eq. (18) have lower and upper bounds at the boundaries of the beam. When the fractional-order derivative (either RL or Caputo) has a lower bound of $-\infty$ the solution kernel of the fractional wave equation can be chosen in the form of exponential functions and we have [38]:

$$ {}^{C,RL}_{-\infty}D^{\alpha}_{x}[\mathrm{e}^{bx}] = b^{\alpha}\mathrm{e}^{bx} \tag{22} $$

When lower bounds other than $-\infty$ are chosen, then solution kernels based on Mittag–Leffler functions are appropriate. However, under proper assumptions for the interval of the fractional derivative both kernels satisfy the same dispersion relations [38]. Similar comment holds for the upper bound. In this study, we choose the exponential kernels given their simplicity and computational efficiency. Using the fractional-order derivative of the exponential given in Eq. (22), we obtain the complete form of the dispersion relations for transverse waves in the fractional-order beam as:

$$ \tilde{\lambda} = \mathrm{e}^{\frac{2\pi \mathrm{i}}{1+\alpha}} \left[\omega^2 \tilde{l}^{2(1-\alpha)} \frac{\tilde{\rho}\tilde{A}}{\tilde{E}\tilde{I}} \right]^{\frac{1}{2(1+\alpha)}} \tag{23} $$

The fractional-order α for the periodic beam can now be obtained by insisting that the wave number obtained through Eq. (23), for a given frequency, is equal to the wave number $\tilde{\lambda}$ obtained using the classical beam theory in Sect. 2, at the same frequency. Recall that the constant $\tilde{l}$ is introduced to ensure dimensional consistency of the formulation and hence, we assume that $\tilde{l} = 1\mathrm{m}$ similar to [38]. These assumptions lead to the following expression for α:

$$ \alpha = \left[\frac{\log\left(\omega^2 \tilde{\rho}\tilde{A}/\tilde{E}\tilde{I}\right)}{\log\left(-\tilde{\lambda}^2\right)} \right] - 1 \tag{24} $$

Note that the propagating component of the wave number for transverse waves in a beam relates to the angular frequency as: $\mathfrak{I}(\lambda) = \omega\rho\mathfrak{A}/\mathfrak{E}\mathfrak{I}$. Using this relation, the expression for α is simplified as:

$$ \alpha = 4\left[\frac{\log|\mathfrak{I}(\lambda)|}{\log\left(-\tilde{\lambda}^2\right)} \right] - 1 \tag{25} $$

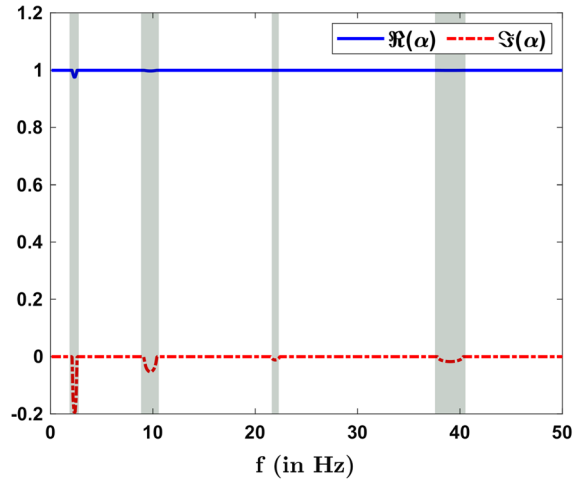

Fig. 4 The plot of the fractional-order α for the aluminum-brass periodic beam as a function of frequency. The fractional-order is equal to 1 for frequencies in the pass-bands, while the order is complex valued for frequencies within the band-gaps of the periodic structure

It is immediate that the fractional-order formulation for the periodic beam results in a variable-order α, where α is a function of the angular frequency ω. Note that for obtaining the value of α, the wave number $\tilde{\lambda}$ corresponding to the unfolded propagating wave solution should be chosen. By using the properties of the periodic beam given in Table 1, the numerically obtained wave numbers in Fig. 2, and the expression for the order given in Eq. (25), we obtain the fractional-order for the periodic beam. The plot of the fractional-order is given in Fig. 4.

We make a few remarks concerning the nature of the fractional-order. First, as evident from Fig. 4, the fractional-order model of the periodic beam results in a complex frequency-dependent order. We emphasize that this characteristic of the fractional-order formulation is independent of the choice of the material and geometric parameters of the periodic beam. Rather, the nature of the order (real or complex) is dependent on the dispersion characteristics of the beam. This behavior of the fractional-order model is related to the characteristics of differential operators with complex orders. As shown in [38, 56, 57], a complex order derivative enables a frequency-dependent modulation of both phase and amplitude of the different harmonic components, therefore allowing for virtually unrestricted matching capabilities for the dispersion relations. Further, it appears from Fig. 4 that the order is a

complex number for band-gap frequencies while, the order is a real number ($\alpha = 1$) for band-pass frequencies. This is consistent with the physics of the problem since $\alpha = 1$ is indicative of propagating waves [41]. In the band-gaps, $\Re(\alpha) <$ and $\Im(\alpha) <$. $\Re(\alpha) <$ indicates that flexural waves in the periodic beam decay spatially, which is again consistent with the fact that this frequency is located within a band-gap. Additionally, as shown in [38], $\Im(\alpha) <$ indicates a frequency-dependent modulation of the phase of the beam response.

5 Steady-state response of the fractional-order beam

We use the fractional model parameters derived in Sect. 4 within the fractional-order beam model to analyse the response of the periodic beam. Given the complex differ-integral nature of the beam governing equations in Eq. (18) we adopt a numerical strategy to solve the governing equations. More specifically, we use the fractional-order finite element method (f-FEM) developed in [48] to simulate the response of the periodic beam. However, certain modifications are necessary because the definition of the RC derivative adopted in this study (see Eq. (14)) is different from [48]. Additionally, the f-FEM proposed in [48] was developed for fractional differential equations (FDEs) with real-valued orders, while the order of the fractional-model for the periodic beam is complex valued. In the following, we briefly discuss the main features of the f-FEM and then the corresponding numerical results.

5.1 Fractional finite element method (f-FEM)

Analogously to classical FEM, the f-FEM is formulated starting from a discretized form of the total potential energy functional given in Eq. (16). The domain $\Omega = [0, L]$ is divided into N_e finite elements denoted as Ω_i^e with $i = \{1, \ldots, N_e\}$ such that $\cup_{i=1}^{N_e} \Omega_i^e = \Omega$ and $\Omega_j^e \cap \Omega_k^e = \emptyset \forall j \neq k$. The transverse displacement at any point $x \in \Omega_i^e$ is evaluated by interpolating the corresponding nodal degrees of freedom of Ω_i^e as:

$$\tilde{w}(x) = [\hat{N}(x)]\{W_i^e\} \tag{26}$$

where, $[\hat{N}(x)]$ is a matrix containing the interpolation functions and $\{W_i^e\}$ is a vector containing the nodal displacement variables of the element Ω_i^e. From the definition given in Eq. (13), the fractional-order axial strain in the beam is expressed as [48]:

$$\begin{aligned}\tilde{\epsilon}(x,z) &= -zD_x^{\alpha}\left(\frac{\partial \tilde{w}}{\partial x}\right) = \frac{-z}{2\Gamma(1-\alpha)} \\ &\quad \left[\int_0^L \mathcal{A}(x,x',\alpha)[B(x')][\tilde{\mathcal{C}}(x,x')]\mathrm{d}x'\right]\{W\} \\ &= -z[\tilde{B}(x)]\{W\}\end{aligned} \tag{27}$$

where x' is a dummy variable used for convolution along the $\hat{x}$ axis, and $\{W\}$ denotes the global degrees of freedom vector. $\mathcal{A}(x, x', \alpha) = 1/|x - x'|^{\alpha}$ denotes the kernel of the fractional-order derivative. Further, the matrix $[B(x')]$ is expressed as:

$$[B(x')] = \frac{\mathrm{d}^2[\hat{N}(x')]}{\mathrm{d}x'^2} \tag{28}$$

Further, $[\tilde{\mathcal{C}}(x, x')]$ is a connectivity matrix that is used to attribute the nonlocal contributions from the different elements in the horizon of x to the corresponding nodes of those elements. In order to correctly account for these nonlocal contributions from the elements in the horizon, we transform the nodal values $\{W_{x'}^e\}$ into $\{\mathrm{W}\}$ using connectivity matrices in the following manner:

$$\{W_{x'}^e\} = [\tilde{\mathcal{C}}(x, x')]\{W\} \tag{29}$$

The connectivity matrix $[\tilde{\mathcal{C}}(x, x')]$ is designed such that it is non-zero only if the point x' lies in the nonlocal horizon of x. It is immediate to see that these matrices activate the contribution of the nodes enclosing x' for the numerical evaluation of the convolution integral in Eq. (27).

The expression for the fractional-order strain in Eq. (27) is used along with the nonlocal stress given in Eq. (15) to obtain the total deformation energy of the beam as:

$$\mathcal{U} = \frac{1}{2}\{W\}^T[\tilde{K}]\{W\} \tag{30}$$

where the nonlocal stiffness matrix $[\tilde{K}]$ is given as:

$$[\tilde{K}] = \tilde{E}\tilde{I}\int_0^L \{\tilde{B}(x)\}^T\{\tilde{B}(x)\}\mathrm{d}x \tag{31a}$$

Note that the use of the connectivity matrix in Eq. (27) results in the fact that the global stiffness matrix $[\tilde{K}]$ is obtained directly in the global form, hence not requiring a separate assembly process for the element stiffness matrices. As discussed in [48], owing to the existence of cross-stiffness matrices, the assembly of the element stiffness matrices in a nonlocal FEM requires care and it is not as immediate as the case of a local FEM. Although it might appear that this assembly strategy would require the use of larger (global) matrices, we emphasize that simple principles of connectivity are used to avoid the multiplication of large sparse matrices in Eq. (27), similar to what is done in local FEM. Note that the FEM also involves the numerical integration of the nonlocal stiffness matrix $[\tilde{K}]$. The specific details of the numerical integration procedure are extensive and can be found in [48].

The final algebraic equations describing the FE model of the fractional-order Euler–Bernoulli beam are now obtained by using the extended Hamilton's principle as:

$$[\tilde{M}]\{\ddot{W}\} + [\tilde{K}]\{W\} = \{F_T\} \tag{32}$$

where the mass-matrix ($[\tilde{M}]$) and the force vector ($\{F_T\}$) of the fractional-order beam are the same as obtained in classical FEM for beams [48, 49]. The solution of the above algebraic equations gives the nodal generalized displacement coordinates. Regarding the f-FEM for the equivalent fractional-order system for the periodic beam, it is convergent for complex orders. More specifically, it was observed that convergence was achieved when the ratio $N_e/L > 10$. This is in contrast to the Grunwald-Letnikov finite difference formula in [39], which was divergent for fractional domains with a complex order. Second, given that we obtain complex values of the order for frequencies with the band-gaps, the f-FEM would require the computation of a complex valued Gamma function (see Eq. (27)). In order to compute the complex valued Gamma function we adopted the algorithm proposed in [58].

5.2 Numerical results and discussion

The f-FEM was applied to analyse the dynamic response of the fractional-order beam. We consider only the section of the infinite periodic beam in the positive portion of the $\hat{x}$ axis and apply a driving condition consisting of a sinusoidal transverse displacement $\tilde{w}(0,t) = W_0 \sin(\Omega_0 t)$ at $x = 0$ as shown in Fig. 5. At the steady-state, we assume a general response in the form $\{W\} = \{W_0\}\sin(\Omega_0 t)$, where $\{W_0\}$ is the steady-state amplitude. By substituting the previous ansatz for $\{W\}$ in the FE Eq. (32), we obtain:

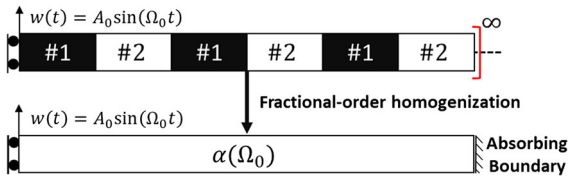

Fig. 5 The infinite bi-layer periodic beam converted into a homogeneous fractional-order beam. The right hand side of the beam is treated with absorbing boundary conditions in order to simulate the infinite beam during the steady state analysis. For the steady state analysis, the response of the periodic beam and its fractional-order counterpart are analyzed following the application of a sinusoidal displacement applied at the left hand side

$$\{W_0\} = \left[[\tilde{K}] - \Omega_0^2[\tilde{M}]\right]^{-1}\{F_T\} \tag{33}$$

Note that, given that the solution is obtained via f-FEM, the initially infinite domain must be truncated. In order to simulate an infinite domain, the truncated end must be complemented with an absorbing boundary condition (that prevents unwanted reflections). The absorbing boundary condition was implemented according to [59].

To demonstrate the capability of the fractional-order formulation we considered the following loading cases: (1) **Loading #1**: the driving angular frequency $\Omega_0 = 5$ rad/s lies in the first pass-band; (2) **Loading #2**: the driving angular frequency $\Omega_0 = 15$ rad/s lies in the first band-gap; (3) **Loading #3**: the driving angular frequency $\Omega_0 = 40$ rad/s lies in the second pass-band; and (4) **Loading #4**: the driving angular frequency $\Omega_0 = 61$ rad/s lies in the second band-gap. The fractional-order α for these cases are obtained using Eq. (25) and are found to be 1, $0.97 - 0.19$i, 1, and $0.99 - 0.05$i, respectively. As expected, the order is an integer for the frequency within the pass-band, while it is complex for the frequency within the band-gap. We expect that the response of the beam is periodic for loading #1 and attenuated for loading #2. The results obtained for the four loading cases defined above are shown in Fig. 6 where they have been compared

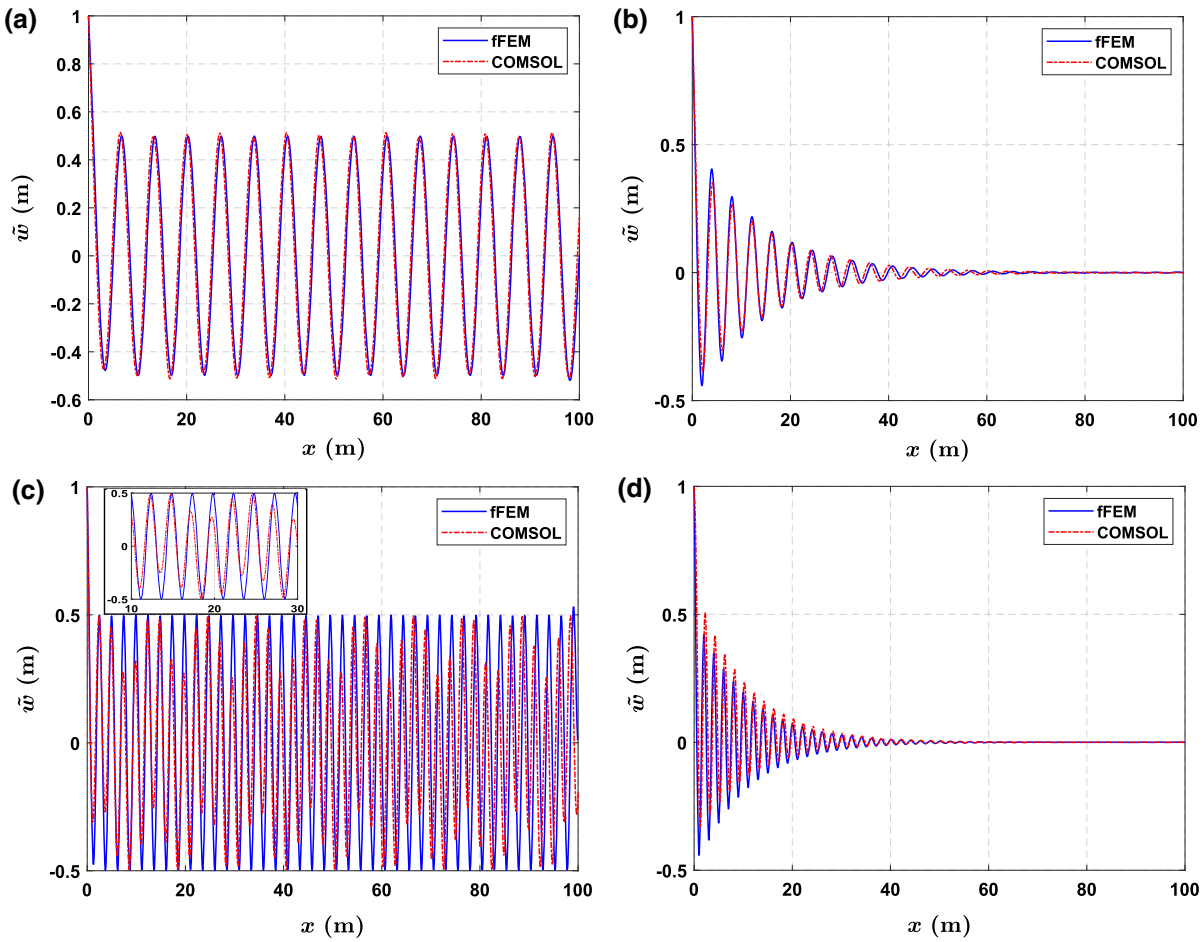

Fig. 6 The steady state response obtained obtained using the fractional order governing equation for the aluminum-brass periodic beam solved via the f-FEM method. For the different cases, the forcing frequency of the external load is within the **a** first pass-band: loading #1, **b** first band-gap: loading #2, **c** second pass-band: loading #3, and **d** second band-gap: loading #4. The inset in **c** provides a zoomed in view of the response of the beam from $x = 10$ m to $x = 30$ m

against numerical simulations obtained using the commercial FE software COMSOL.

As evident from Fig. 6, the match between the results obtained via the fractional-order formulation and the classical results, when the driving angular frequency lies within the first pass-band and first band-gap frequencies (loading #1 and loading #2), are excellent. The maximum error (ℓ^∞ norm) obtained between the f-FEM and COMSOL results are 1% and 2% in the loading (1) and (2), respectively. For the loading #3 where the driving angular frequency lies within the second pass-band, the f-FEM result matches the phase of the COMSOL result, but does not match the amplitude locally. This type of behavior is not unexpected because the frequency is near the long wavelength limit and the response is increasingly dominated by scattering effects. Further, recall that for band-pass frequencies, the order of the fractional system is $\alpha = 1$ and for $\alpha = 1$, the fractional-order beam formulation reduces to the classical Euler–Bernoulli beam formulation with homogenized material properties (see Eq. (25)). Like other homogenization techniques, the proposed fractional homogenization model cannot capture localized effects due to wave scattering. In order to capture the localized effects, the fractional methodology would need to be modified. It is hypothesized that the localized effects associated with the short wavelength limit could be captured by utilizing a spatially-variable fractional order. Note, however, the good

agreement between the f-FEM and the COMSOL results for loading #4 where the driving angular frequency lies within the second band-gap. The maximum error (ℓ^∞ norm) obtained between the f-FEM and COMSOL result is merely 7% in this case. Again, the amplitudes of the two curves do not match due to localization at high frequencies, but the fractional model did successfully capture the attenuating flexural displacement within the band-gap. This is a key feature that most classical homogenization approaches cannot capture accurately.

Recall that the proposed technique is effectively a homogenization approach and like most homogenization methods (except for some recently developed high-frequency homogenization techniques), it is locally accurate only for long wavelengths. When approaching short wavelength regimes, local interference effects due to forward propagating and backscattered waves cannot be accurately captured. Nevertheless, this approach is able to correctly capture the wave attenuation as well as the proper spatial phase for band-gap frequencies. These results highlight the robustness of the fractional-order formulation in capturing the response of the periodic beam particularly at band-gap frequencies, where classical homogenization techniques fail to capture the spatial attenuation of the flexural waves [38]. The results presented above for driving frequencies within the first and second band-gap allow us to make some remarks on the nature of the fractional-order model predictions for higher-order band-gaps. For higher-order band-gaps, it is expected that the fractional-order model presented in this study will capture attenuation due to the complex valued fractional-order (see Fig. 4). However, there would be an increasing mismatch in the amplitude of the response due to the inability of the fractional-order model to capture the localized scattering effects. In this regard, depending on the specific application, the latter aspect may or may not be a disadvantage. As an example, if the objective is to simulate the response of a solid with an embedded slab of the periodic medium (e.g. a periodic 1D beam embedded in an otherwise homogeneous beam), the detailed response inside the periodic medium might not be of interest. Note that this comment is applicable to homogenized models in general and it is neither a consequence nor a peculiarity of the fractional order modeling.

We conclude observing that, in view of the above described characteristics, the homogenized fractional model may provide a powerful alternative route to develop homogenization approaches. In this regard, we note some advantages of the fractional-order approach over classical (integer-order) high-frequency homogenization techniques. Recall that the location of the band-gaps in high-frequency homogenization approaches is computed by solving the eigenvalue problem corresponding to a unit cell subject to quasi-periodic boundary conditions, obtained via asymptotic multiple scale representation of the elastodynamic equation. The computation of this eigenvalue problem is often limited by the computational capabilities of the eigen solver and becomes progressively more complex as a higher number of terms is used within the multiscale expansion. The combination of this aspect with the need for a local approximation of the periodic structure's dispersion curves (near the band-gaps) leads to a limitation on the accuracy of high-frequency homogenization approaches. On the other side, we note that the high-frequency homogenization approach is theoretically more rigorous than the fractional-order approach proposed in this work. Nevertheless, we also highlight that this work was intended to explore the feasibility and the potential of fractional-order homogenization techniques for the simulation of periodic systems, and it should not be considered as indicative of optimal performance. Indeed, it is possible to envision that the performance of the proposed method could be further improved by taking full advantage of the spectrum of opportunities offered by fractional operators such as, for example, extending the method using either variable-order [60] or distributed-order operators [25]. Variable-order operators are well-equipped to capture spatially-varying microstructures [60] and distributed-order operators can capture multiscale response [25].

6 Conclusions

This study presented a preliminary assessment on the application of fractional calculus to the homogenization of heterogeneous structures. In particular, the formulation of a fractional-order homogenization technique for the analysis of 1D periodic beams was presented and shown to be capable of overcoming the

classical long wavelength limit typical of low-frequency techniques. At a mathematical level, the differ-integral nature of the space-fractional operators was exploited to convert the classical integer-order differential equation with spatially-variable coefficients, governing the flexural response of beams, into a fractional differential equation with constant coefficients. By assuming a nonlocal horizon equal to the length of the beam, the order of the fractional model was derived by imposing the equivalence of the dispersion behavior with the initial heterogeneous beam. The procedure yielded a complex-valued and frequency-dependent order whose real and imaginary parts are related to the decay and to the frequency modulation of the amplitude and phase of the wave propagating in the medium. A fractional-order finite element method (f-FEM) was developed in order to numerically solve the complex-valued and fractional-order governing equations. The consistency of this numerical method was a direct result of the self-adjoint, well-posed, and positive definite nature of the fractional-order system. The f-FEM outperforms, particularly in terms of stability, previously used methods based on finite difference schemes. The fractional-order framework was validated, at both band-pass and band-gap frequencies, by direct comparison against the response of a periodic beam solved via the traditional finite element method based on integer-order equations. The ability of the fractional order models to capture the attenuation within the first few band-gaps is a strength of the proposed method over classical low-frequency homogenization techniques that cannot capture the spatial decay of waves unless resorting to the addition of artificial and unrealistic damping terms.

In conclusion, the fractional-order method provides an interesting alternative route to extend the range of applicability of homogenization techniques beyond the classical long wavelength limit. This aspect suggests that fractional-order mathematics could serve as the basis to develop a new generation of high-frequency homogenization methods, potentially capable of combining the strengths of both low- and high-frequency methods. We finally highlight that the fractional-order homogenization technique developed in this study is very general in nature. Although it was applied to one-dimensional periodic structures, it is anticipated that this technique could be extended to higher dimensional periodic systems.

Acknowledgements The authors gratefully acknowledge the financial support of the National Science Foundation (NSF) under Grants MOMS #1761423, and the Defense Advanced Research Project Agency (DARPA) under Grant #D19AP00052. J.P.H. acknowledges the financial support of the National Defense Science and Engineering Graduate Fellowship (NDSEG). The content and information presented in this manuscript do not necessarily reflect the position or the policy of the government. The material is approved for public release; distribution is unlimited.

Declarations

Conflict of interest The authors declare that they have no conflict of interest.

References

1. Ao X, Chan CT (2008) Far-field image magnification for acoustic waves using anisotropic acoustic metamaterials. Phys Rev E 77:025601
2. Zhang S, Xia C, Fang N (2011) Broadband acoustic cloak for ultrasound waves. Phys Rev Lett 106:024301
3. Zhu H, Semperlotti F (2013) Metamaterial based embedded acoustic filters for structural applications. AIP Adv 3:092121
4. Zhu H, Semperlotti F (2015) Phononic thin plates with embedded acoustic black holes. Phys Rev B 91:104304
5. Zhu H, Patnaik S, Walsh TF, Jared BH, Semperlotti F (2020) Nonlocal elastic metasurfaces: enabling broadband wave control via intentional nonlocality. Proc Natl Acad Sci 117:26099–26108
6. Bostani A, Webb JP (2011) A model-order reduction method for the passband and stopband characteristics of periodic structures. In: 2011 41st European microwave conference. IEEE, pp 167–170
7. Bostani A, Webb JP (2012) Finite-element eigenvalue analysis of propagating and evanescent modes in 3-d periodic structures using model-order reduction. IEEE Trans Microw Theory Tech 60:2677–2683
8. Navarro EA, Gimeno B, Cruz JL (1993) Modelling of periodic structures using the finite difference time domain method combined with the floquet theorem. Electron Lett 29:446–447
9. Sigalas MM, Garcıa N (2000) Theoretical study of three dimensional elastic band gaps with the finite-difference time-domain method. J Appl Phys 87:3122–3125
10. Cheng ZB, Xu YG, Zhang LL (2015) Analysis of flexural wave bandgaps in periodic plate structures using differential quadrature element method. Int J Mech Sci 100:112–125
11. Cheng ZB, Shi ZF, Mo YL (2018) Complex dispersion relations and evanescent waves in periodic beams via the extended differential quadrature method. Compos Struct 187:122–136
12. Bao G (1995) Finite element approximation of time harmonic waves in periodic structures. SIAM J Numer Anal 32:1155–1169

13. Duhamel D, Mace BR, Brennan MJ (2006) Finite element analysis of the vibrations of waveguides and periodic structures. J Sound Vib 294:205–220
14. Cao Y, Hou Z, Liu Y (2004) Convergence problem of plane-wave expansion method for phononic crystals. Phys Lett A 327:247–253
15. Shi S, Chen C, Prather DW (2004) Plane-wave expansion method for calculating band structure of photonic crystal slabs with perfectly matched layers. JOSA A 21:1769–1775
16. Yu W, Tang T (2007) Variational asymptotic method for unit cell homogenization of periodically heterogeneous materials. Int J Solids Struct 44:3738–3755
17. Craster RV, Kaplunov J, Pichugin AV (2010) High-frequency homogenization for periodic media. Proc R Soc A Math Phys Eng Sci 466:2341–2362
18. Antonakakis T, Craster RV, Guenneau S (2013) High-frequency homogenization of zero-frequency stop band photonic and phononic crystals. New J Phys 15:103014
19. Manevitch LI, Andrianov IV, Oshmyan VG (2013) Mechanics of periodically heterogeneous structures. Springer, Berlin
20. Yang M, Ma G, Wu Y, Yang Z, Sheng P (2014) Homogenization scheme for acoustic metamaterials. Phys Rev B 89:064309
21. Podlubny I (1998) Fractional differential equations: an introduction to fractional derivatives, fractional differential equations, to methods of their solution and some of their applications, vol 198. Elsevier, Amsterdam
22. Chatterjee A (2005) Statistical origins of fractional derivatives in viscoelasticity. J Sound Vib 284:1239–1245
23. Magin RL (2010) Fractional calculus models of complex dynamics in biological tissues. Comput Math Appl 59:1586–1593
24. Hollkamp JP, Sen M, Semperlotti F (2018) Model-order reduction of lumped parameter systems via fractional calculus. J Sound Vib 419:526–543
25. Patnaik S, Sidhardh S, Semperlotti F (2021) Towards a unified approach to nonlocal elasticity via fractional-order mechanics. Int J Mech Sci 189:105992
26. Patnaik S, Sidhardh S, Semperlotti F (2020) Fractional-order models for the static and dynamic analysis of nonlocal plates. Commun Nonlinear Sci Numer Simul 95:105601
27. Patnaik S, Sidhardh S, Semperlotti F (2020) Geometrically nonlinear analysis of nonlocal plates using fractional calculus. Int J Mech Sci 179:105710
28. Sidhardh S, Patnaik S, Semperlotti F (2020) Geometrically nonlinear response of a fractional-order nonlocal model of elasticity. Int J Nonlinear Mech 125:103529
29. Lazopoulos KA (2006) Non-local continuum mechanics and fractional calculus. Mech Res Commun 33:753–757
30. Carpinteri A, Cornetti P, Sapora A (2011) A fractional calculus approach to nonlocal elasticity. Eur Phys J Spec Top 193:193
31. Drapaca CS, Sivaloganathan S (2012) A fractional model of continuum mechanics. J Elast 107:105–123
32. Di Paola M, Failla G, Pirrotta A, Sofi A, Zingales M (2013) The mechanically based non-local elasticity: an overview of main results and future challenges. Philos Trans R Soc A Math Phys Eng Sci 371:20120433
33. Sumelka W, Blaszczyk T (2014) Fractional continua for linear elasticity. Arch Mech 66:147–172
34. Sumelka W, Blaszczyk T, Liebold C (2015) Fractional Euler–Bernoulli beams: theory, numerical study and experimental validation. Eur J Mech A Solids 54:243–251
35. Alotta G, Failla G, Zingales M (2017) Finite-element formulation of a nonlocal hereditary fractional-order Timoshenko beam. J Eng Mech 143:D4015001
36. Szajek K, Sumelka W, Bekus K, Blaszczyk T (2021) Designing of dynamic spectrum shifting in terms of non-local space-fractional mechanics. Energies 14:506
37. Zingales M, Failla G (2015) The finite element method for fractional non-local thermal energy transfer in non-homogeneous rigid conductors. Commun Nonlinear Sci Numer Simul 29:116–127
38. Hollkamp JP, Sen M, Semperlotti F (2019) Analysis of dispersion and propagation properties in a periodic rod using a space-fractional wave equation. J Sound Vib 441:204–220
39. Hollkamp JP, Semperlotti F (2020) Application of fractional order operators to the simulation of ducts with acoustic black hole terminations. J Sound Vib 465:115035
40. Szajek K, Sumelka W (2019) Discrete mass-spring structure identification in nonlocal continuum space-fractional model. Eur Phys J Plus 134:1–19
41. Patnaik S, Semperlotti F (2020) A generalized fractional-order elastodynamic theory for non-local attenuating media. Proc R Soc A 476:20200200
42. Benson DA, Wheatcraft SW, Meerschaert MM (2000) Application of a fractional advection–dispersion equation. Water Resour Res 36:1403–1412
43. Fellah ZEA, Chapelon JY, Berger S, Lauriks W, Depollier C (2004) Ultrasonic wave propagation in human cancellous bone: application of Biot theory. J Acoust Soc Am 116:61–73
44. Meerschaert MM, McGough RJ (2014) Attenuated fractional wave equations with anisotropy. J Vib Acoust 136:050902
45. Buonocore S, Sen M, Semperlotti F (2019) Occurrence of anomalous diffusion and non-local response in highly-scattering acoustic periodic media. New J Phys 21:033011
46. Zhang H, Liu F, Anh V (2010) Galerkin finite element approximation of symmetric space-fractional partial differential equations. Appl Math Comput 217:2534–2545
47. Wang H, Yang D, Zhu S (2015) A Petrov–Galerkin finite element method for variable-coefficient fractional diffusion equations. Comput Methods Appl Mech Eng 290:45–56
48. Patnaik S, Sidhardh S, Semperlotti F (2020) A Ritz-based finite element method for a fractional-order boundary value problem of nonlocal elasticity. Int J Solids Struct 202:398–417
49. Reddy JN (2019) An introduction to the finite element method. McGraw-Hill Education, New York
50. Eringen AC, Edelen DGB (1972) On nonlocal elasticity. Int J Eng Sci 10:233–248
51. Sidhardh S, Patnaik S, Semperlotti F (2021) Thermodynamics of fractional-order nonlocal continua and its application to the thermoelastic response of beams. Eur J Mech A Solids 88:104238
52. Challamel N et al (2014) On nonconservativeness of Eringen's nonlocal elasticity in beam mechanics: correction from a discrete-based approach. Arch Appl Mech 84:1275–1292

53. Lazopoulos KA, Lazopoulos AK (2020) On fractional bending of beams with Λ-fractional derivative. Arch Appl Mech 90:573–584
54. Lazopoulos KA, Lazopoulos AK (2020) On plane Λ-fractional linear elasticity theory. Theor Appl Mech Lett 10:270–275
55. Lazopoulos AK, Karaoulanis D (2021) On Λ-fractional viscoelastic models. Axioms 10:22
56. Makris N, Constantinou MC (1993) Models of viscoelasticity with complex-order derivatives. J Eng Mech 119:1453–1464
57. Love ER (1971) Fractional derivatives of imaginary order. J Lond Math Soc 2:241–259
58. Luke YL (1969) Special functions and their approximations, vol 2. Academic Press, New York
59. Andersen L, Nielsen SRK, Kirkegaard PH (2001) Finite element modelling of infinite Euler beams on kelvin foundations exposed to moving loads in convected co-ordinates. J Sound Vib 241:587–604
60. Jokar M, Patnaik S, Semperlotti F (2020) Variable-order approach to nonlocal elasticity: Theoretical formulation and order identification via deep learning techniques. arXiv: 2008.13582